# Unsteady Surface Pressure Characteristics on Aircraft Components and Far-Field Radiated Airframe Noise

Hanno H. Heller* and Werner M. Dobrzynski†
*Abteilung Technische Akustik DFVLR, Braunschweig, Germany*

**Aircraft wings and landing gears have been identified as primary contributors to airframe noise. An experimental and analytical research program was conducted to determine the relationship of aeroacoustic source mechanisms at the origin and the resulting far-field acoustic radiation for these particular aircraft components. Employing an aerodynamically very clean glider both as test vehicle and test bed, fluctuating surface pressure characteristics were determined in regions that were suspected to be prime source areas—viz, the wing flap trailing edges, and the region of highly turbulent flow impingement, or flow separation, on fairly large models of four-wheel main landing gears. Source characteristics in terms of surface pressure spectra and longitudinal and lateral pressure correlation lengths were used to predict far-field acoustic radiation with results that compared favorably with measured data.**

## Nomenclature

$a$ = ambient speed of sound, m/s
$A$ = correlation area, $m^2$
$D$ = landing gear wheel diameter, m
$D_\omega$ = dipole strength, $m^4/s$
$f$ = frequency, Hz
$F_D$ = fluctuating force, N
$G_1$ = power spectral density, W/Hz
$G_2$ = power spectral density, W/Hz
$G_{1,2}$ = cross spectral density, W/Hz
$k$ = acoustic wave number, $m^{-1}$
$l_x$ = longitudinal (streamwise) correlation length, m
$l_y$ = lateral correlation length, m
$L_p$ = pressure level, dB
$M_\infty$ = freestream (flight) Mach number
$n$ = number of correlated areas within a total radiating area
$p_F$ = rms sound pressure, Pa
$p_S$ = rms surface pressure, Pa
$q_\infty$ = freestream dynamic pressure, Pa
$r$ = distance between source and receiver, m
$U_\infty$ = freestream (flight) velocity, m/s
$\Delta x$ = longitudinal (streamwise) sensor-separation distance, m
$\Delta y$ = lateral sensor-separation distance, m
$Y$ = total wetted span, $Y = n \cdot l_y$, m
$\gamma$ = coherence function, $\gamma = |G_{1,2}| / \sqrt{G_1 \cdot G_2}$
$\delta^*$ = boundary-layer displacement thickness, m
$\eta$ = flap angle relative to the wing chord, deg
$\theta$ = angle between the dipole force axis and the direction of radiated sound, rad
$\Pi$ = sound power, W
$\rho$ = freestream density, $kg/m^3$
$\omega$ = circular frequency, $s^{-1}$

## Problem Statement

THE dominant aeroacoustic mechanisms of airframe noise are intimately related to aerodynamically induced unsteady pressures on aircraft components. Although aircraft wings and landing gears have been identified as major contributors to airframe noise, the physical mechanisms of sound generation by unsteady pressures on these components were not fully understood and quantitative proof of the direct relationship of fluctuating surface pressures and resulting far-field sound radiation was lacking. Theoretical approaches to predict airframe noise usually employed educated guesses on the magnitude, spectral energy distribution, and correlation characteristics of unsteady pressure fields on aircraft surfaces. Precise information on these quantities, however, is necessary to determine the resulting unsteady forces on aircraft components and the subsequent radiation of sound due to these force fluctuations.

To obtain this information, researchers have frequently resorted to wind-tunnel experiments employing elementary shapes, such as flat plates, two-dimensional airfoils, or simple three-dimensional bodies in order to determine surface-pressure characteristics, and, in limited cases, also the resulting far-field acoustic signal. Even with the greatest of care, however, such tests are hampered by two major adversaries, namely tunnel background noise and inherent tunnel flow turbulence. Moreover, there is rarely enough space available in tunnels to extend the measurement distance far enough into the far-field, quite aside from the difficulty of measuring acoustic signals in the presence of turbulent flow. It is questionable therefore, whether results from tests carried out under such unfavorable conditions can be readily applied to the airframe noise problem.

Thus a "clean" experiment was called for where, under realistic conditions, both source characteristics and resulting far-field acoustic spectra could be measured in order to determine the relevance of trailing-edge and landing gear related sources to the complex phenomenon of airframe noise.

The glider – particularly an aerodynamically very clean glider – offers itself as a distinctly qualified test object for airframe noise research. There are several prime advantages, not offered by any other experimental technique. First, a glider represents a "near full-scale" aircraft when compared to typical medium size commercial aircraft. Fairly close to full-scale Reynolds numbers for wing surface flows may be obtained. Typical glider speeds approach commercial aircraft landing approach speeds, the relative motion of source and observer is correctly simulated and, above all, there is no disturbing engine noise.

Thus, in a basic study where surface pressure characteristics on, say, aircraft wing flaps are to be related to a far-field radiated acoustic signal, a glider is an excellent experimental tool. Likewise, a glider is an ideal flying test-bed to investigate

Presented as Paper 77-1295 at the AIAA 4th Aeroacoustics Conference, Atlanta, Ga., Oct. 3-5, 1977; submitted Nov. 2, 1977; revision received July 5, 1978. 
Index categories: Noise; Aeroacoustics.
*Manager. Member AIAA.
†Senior Scientist.

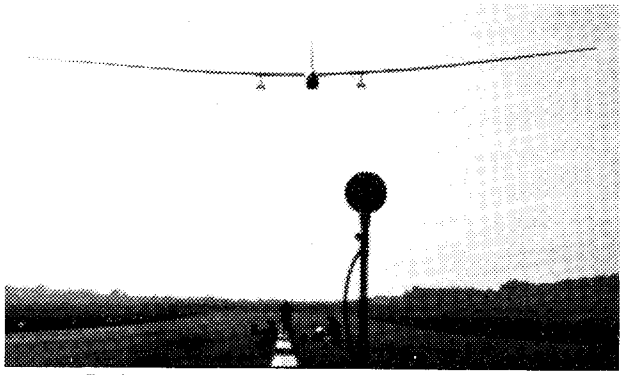

Fig. 1 SB-10 glider approaching the acoustic measurement station.

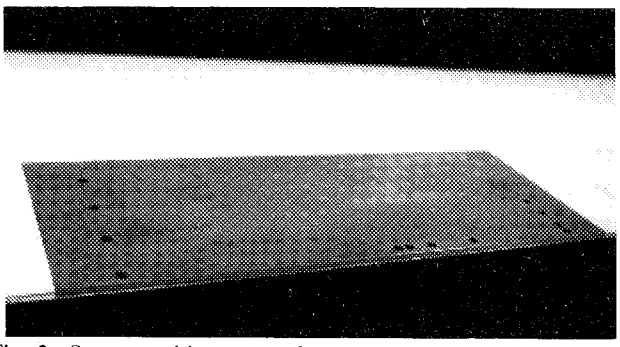

Fig. 2 Sensor positions on and near the glider wing-flap trailing edge.

source and radiation characteristics of aircraft components such as landing gears, when employed as a carrier of appropriate models.

## Experimental Techniques‡

The test aircraft – the Braunschweig Akaflieg SB-10 – is a high-performance glider with an unusually large wing span of 29 m, an average wing chord of 0.8 m, corresponding to a wing aspect ratio of 36.6.[1] The glider approaching the acoustic measurement station is shown in Fig. 1.

There were two series of tests. For the first, the glider was used in its original configuration, and surface pressure spectra were measured by flush-mounted sensors near the trailing edge of the wing flap, arranged both along and across the flow direction. Figure 2 shows the arrangement of the BBN type 382 piezoelectric sensors with a 6.0-mm-diam sensing area. A total of 12 locations covered a lateral center-to-center spacing from 1 cm to 33 cm and a longitudinal (steamwise) spacing from 2 cm to 11 cm.

Due to the limited space within the two-seat glider cockpit, the copilot was able to operate only one NAGRA two-track tape recorder for data acquisition. Data were acquired at flight speeds of 28, 35, 42, 49, and 56 m/s and for flap settings of −10, 0, +10, +40, +70, and +85 deg, thus covering a range of typical cruise and landing approach conditions and configurations.

For the second test series, two main landing gear models (synthesized from those of large commercial aircraft such as DC-10, L-1011, or B747) of scale 1:4 were attached to the wings of the SB-10 (Fig. 3). A total of four sensors (BBN type 376) – two in a front wheel at both sides, two more in an aft wheel again at both sides – were installed flush within the surrounding surface (Fig. 4). By turning the wheels, three effective locations of the sensors with respect to the impinging mean flow direction (i.e., 0, 90, and 135 deg) were obtained, thus covering regions of attached and separated flow. Thus, areas of particularly high fluctuating pressure intensities that

‡All spectra are presented in terms of ⅓-octave-band levels unless otherwise noted. Levels are referenced to 20 $\mu$Pa.

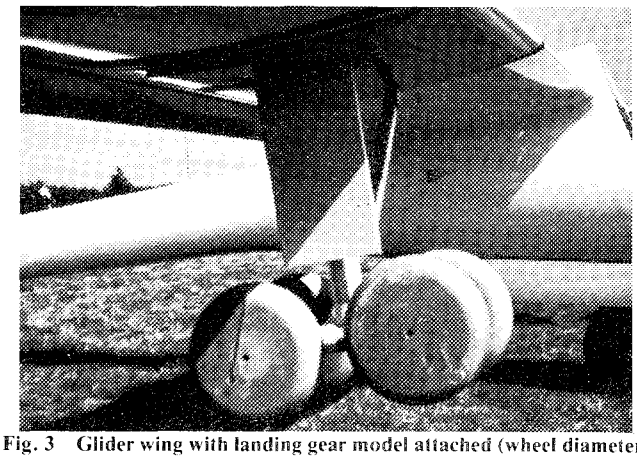

Fig. 3 Glider wing with landing gear model attached (wheel diameter 0.27 m).

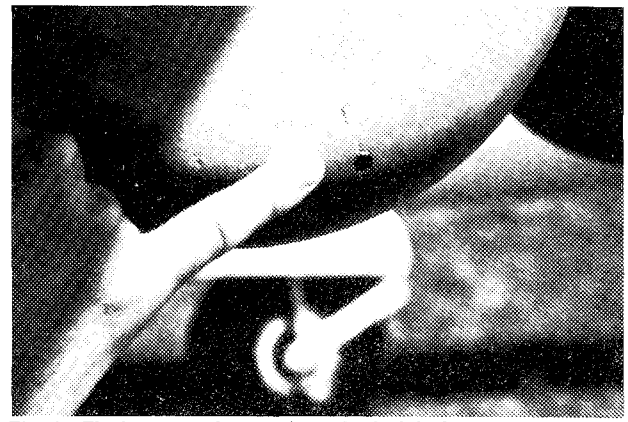

Fig. 4 Flush-mounted sensor in a wheel of the landing gear model.

might act as potent sound sources could be identified. Surface spectra were acquired for flight speeds from 28 to 56 m/s. Acoustic data were again recorded by an onboard two-track tape recorder. For both test series, glider surface pressure spectra were analyzed either in ⅓ octaves or in 10-Hz narrow bands.

Far-field noise radiated from the SB-10, either in its clean configuration or with landing gear models attached, was measured by ground-located Brüel and Kjaer 1-in.-diam condenser microphones. When measuring unweighted sound pressure levels over a large frequency range (0.1 – 10 kHz) the microphone height above ground of 1.2 m as used in certification measurements is particularly unfavorable. Thus, two techniques were employed, one where the microphones were laid flat on the concrete surface of the runway, another where the microphones were elevated 5 m above ground. By using data from both sets of microphones, one can avoid the region of large level variations due to ground reflection effects and employ well defined corrections of either −6 dB for the ground-located microphones or −3 dB for the elevated microphones. It should be mentioned that burying the microphones into a hard and solid surface with their diaphragms flush with the surrounding surface would be ideal, requiring a −6-dB correction for all frequencies; however, such a setup is usually not feasible.

Flight height and speed were determined from the ground through a high-speed (64-frames/s) camera. Far-field ⅓-octave band spectra were composed from individual ⅓-octave band time histories.

## Trailing-Edge Aeroacoustic Source Characteristics and Far-Field Radiation

The wing profile of the SB-10 glider pertains to the Wortmann-Series with classification FX 62135. At a flight speed of

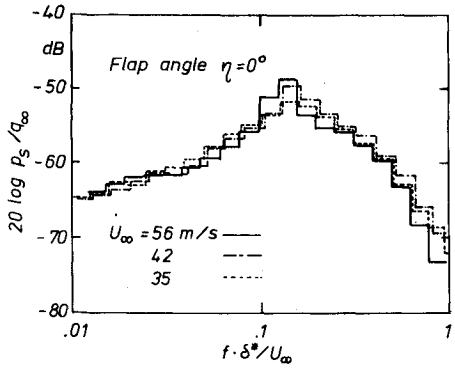


**Fig. 5 Typical normalized wing-flap trailing-edge surface pressure spectra measured on the SB-10 glider (not corrected for finite transducer size).**

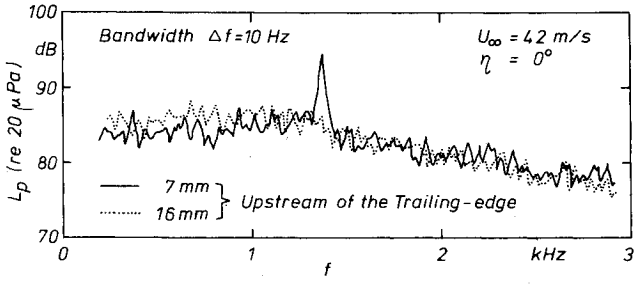


**Fig. 6 Narrowband wing-flap surface pressure spectra measured at two locations upstream of the trailing edge (flap angle $\eta = 0$ deg).**

50 m/s, the chord-based Reynolds number is about 3.3 million. Within the speed range investigated ($28 < U_\infty < 56$ m/s) flow transition occurs at the 50-60% chord position. Thus, surface flow is fully turbulent under all flight conditions by the time it reaches the trailing edge.

### Fluctuating Surface Pressure Data

Figure 5 shows typical surface pressure spectra at a location 1.2 sensor diameters upstream of the trailing edge at a flap angle of $\eta = 0$ deg. Surface pressures are normalized with the freestream dynamic pressure, frequencies are nondimensionalized on a Strouhal number basis. Since only calculated,§ rather than measured, displacement thicknesses were available, no finite transducer size correction is applied. The measured trailing-edge spectra (with the exception of the maximum near $f \cdot \delta^*/U_\infty = 1.2$, which may indicate the presence of a discrete-frequency flow-shedding phenomenon at the trailing edge, to be discussed) correspond to those that have been measured for attached turbulent boundary layers with equal physical properties (i.e., flap-angle, displacment thickness, Reynolds number). Hence, the presence of a boundary discontinuity seems not to affect the properties of the approaching boundary-layer flow, which are in their entirety determined by the upstream flow history. The edge, of course, is instrumental in the sound generating process, leading to an aeroacoustic dipole mechanism due to flow spillage past an edge.

Narrowband spectral analysis of trailing-edge pressure fluctuations confirm the presence of a discrete-frequency flow phenomena and indicate strongly periodic shedding processes even for turbulent boundary-layer conditions. Evidently the phenomenon is localized at the very trailing edge, since upstream measurements do not show any periodic flow behavior (Fig. 6). Tones in the spectra cannot be normalized on a Strouhal number basis with the displacement thickness as length parameter. However, they were observed consistently

§The turbulent boundary-layer displacement thickness was calculated to be about 5 mm at the trailing edge for all speeds investigated and flap angles $-10 < \eta < 10$ deg.

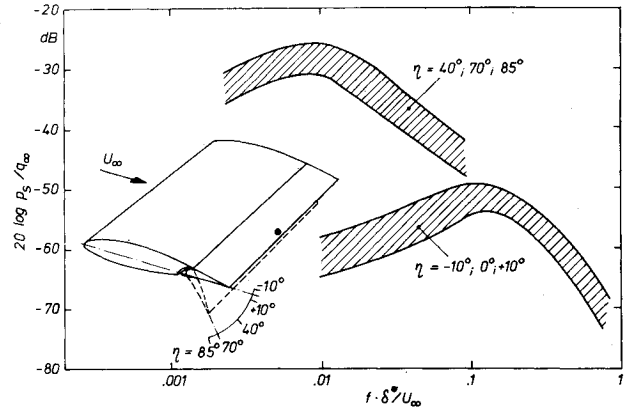


**Fig. 7 Wing-flap trailing-edge surface pressure spectra for different flap deflections (surface pressures not corrected for finite transducer size).**

and most pronounced for negative (i.e. upward) flap settings in the immediate vicinity of the trailing edge. Further upsteam, as also observed by Hahn,[2] the tones were immersed in the broadband noise level.

The typical data scatter that occured for nominally identical flight conditions (i.e., ±0.5 dB) and, more pronounced, even for different sensor positions in the spanwise direction (i.e. ±2 dB) is illustrated in Fig. 7. Data for flap settings of $40 < \eta < 85$ deg fall in a ±3-dB band, with levels some 25 dB higher than for the low-angle flap settings. The flow in all likelihood was fully separated for the larger flap deflections.

### Pressure-Field Correlation Characteristics

Postulating that the total radiating area for trailing-edge noise can be represented by a number of incoherently radiating surface pressure "correlation areas," both the longitudinal (streamwise) and lateral correlation lengths as a function of frequency needed to be determined. Figure 8 shows the longitudinal pressure field correlation in terms of a coherence vs a normalized sensor distance as measured by Panton[3] on a flat portion of a glider fuselage. This is a different representation than that used by Panton, to illustrate that there is, expectedly, no parameter combination that can collapse pressure field coherence data into one curve. On the one hand, the coherence of the fluctuating pressures increases steadily towards unity with decreasing sensor separation distance. On the other hand, for a given sensor separation distance, the coherence reaches a maximum at some frequency. Thus, there should exist a limiting frequency below which no correlation length can be defined by integrating the curves shown in Fig. 8.

Before determining this limiting frequency, Panton's data, together with data obtained in the present study in the wing-flap trailing-edge area, and data by Schloemer[4] and by Bull[5] are shown in a representation employing a linear abscissa scale (Fig. 9). The data need not necessarily fall all upon one curve, since Panton's data were taken on a flat portion of a glider fuselage, while both Schloemer and Bull obtained their data in wind tunnels on straight surfaces. Since "coherence vs normalized sensor separation distance" is a continuous function, correlation lengths can only be defined by a mean value, i.e. the integral of $\gamma$ vs $f \cdot \Delta x/U_\infty$. Numerical integration of the curve drawn through the SB-10 glider wing-flap data yields a longitudinal correlation length of $l_x = 0.72\ U_\infty/f$. Corresponding information on the lateral coherence as obtained in the present study, and by Schloemer[4] and Bull[5] are shown in Fig. 10, the SB-10 data yielding a correlation length of $l_y = 0.26\ U_\infty/f$.

From Fig. 8 it can be seen that the curves tend to collapse at frequencies above the frequency of the maximum coherence, but fan out at lower frequencies. Evidently, the limiting nondimensional frequency is given by that frequency where each curve branches off. The corresponding nondimensional

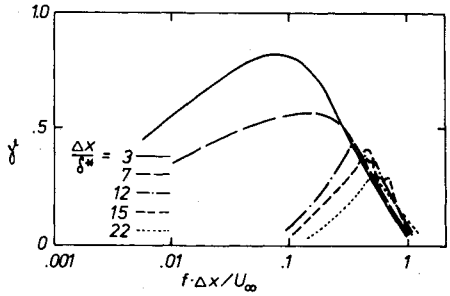


**Fig. 8 Longitudinal coherence of surface pressure fluctuations as a function of normalized sensor-separation distance measured on a glider fuselage (after Panton[3]).**

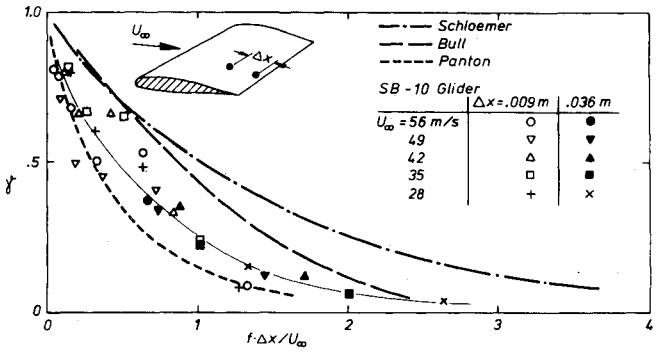


**Fig. 9 Longitudinal coherence of surface pressure fluctuations as a function of normalized sensor-separation distance.**

frequencies taken from data obtained by Panton,[3] Bull,[5] and also by Bhat,[6] who measured longitudinal pressure field coherence on a B737 aircraft fuselage, are plotted in Fig. 11 both for longitudinal and lateral coherence. Equivalent results from measurements reported here correspond to relatively low ratios of $\Delta x/\delta^*$ and therefore to frequencies below some 400 Hz. Because of possible vibrational excitation of the pressure sensors in this low-frequency range, relevant data are not included in Fig. 11. There exists, expectedly, a substantial data scatter. However, a straight line of unity slope can be drawn through the data points, yielding a simple expression for the limiting frequency for both longitudinal and lateral correlation lengths of $f_{\text{limit}} \simeq 0.04\ U_\infty/\delta^*$. Hence, the previously derived longitudinal and lateral correlation lengths are only valid for frequencies above those defined by the limiting frequency. Considering a test condition where the glider flies with an airspeed of 50 m/s, the limiting frequency would be aobut 400 Hz.

### Prediction of Far-Field Sound Radiation from Trailing-Edge Fluctuating Pressure Field

Generation of "edge noise" through the interaction of attached turbulent surface flow and a (wing flap) trailing edge, can be thought of as being the result of the hydrodynamic acceleration of fluid flow elements at – or rather just downstream of – the trailing edge due to the fluctuating pressure difference between the upper and lower trailing-edge surface. The unsteady force resulting from this unsteady fluid-element acceleration causes equal and opposite reactive forces on the trailing edge. Such forces can be measured in terms of fluctuating pressures acting on appropriate surface correlation areas. It should be realized that the fluctuating surface forces on the trailing edge do not generate sound, but rather the unsteady hydrodynamic processes just downstream of the trailing edge, which are, in turn, intimately related to the phenomena on the trailing edge, where measurements are possible.

On the basis of these considerations it is fairly straightforward to develop an analytical expression for trailing-edge sound power radiation, or, more appropriately, of the

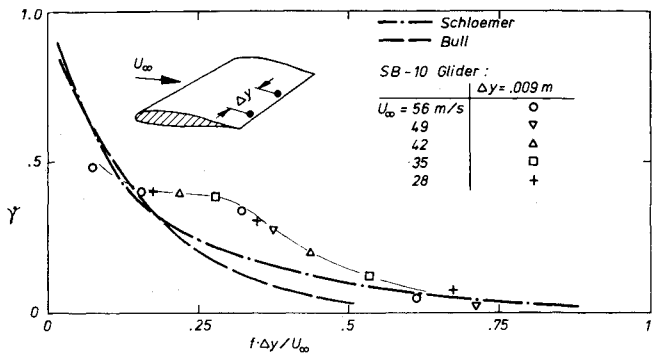


**Fig. 10 Lateral coherence of surface pressure fluctuations as a function of normalized sensor-separation distance.**

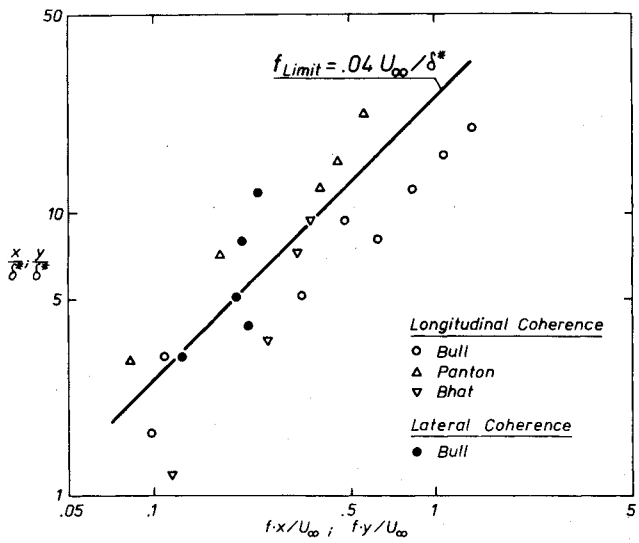


**Fig. 11 Relationship between the frequency limiting the normalization of pressure field coherence functions and the corresponding flow parameters.**

relationship between surface pressure spectrum and far-field radiated sound pressure spectrum.

Sound power $\pi$ radiated from a simple dipole source of strength $D_\omega$ is given by Morse and Ingard[7] as

$$\Pi(\omega) = \frac{\rho\omega^4}{12\pi a^3}\,|D_\omega|^2 \tag{1}$$

The mean square force $\overline{|F_D^2(\omega)|}$ necessary to oscillate a fluid element of characteristic dimension $l$ is

$$\overline{|F_D^2(\omega)|} = \rho^2\omega^2\,|D_\omega|^2/9 \tag{2}$$

provided $k \cdot l \ll 1$, where $k$ is the wave number. Insertion of Eq. (2) into Eq. (1) yields an expression for sound power as function of force fluctuation, i.e.,

$$\Pi(\omega) = \frac{3}{4}\,\frac{\omega^2\,\overline{|F_D^2(\omega)|}}{\pi\rho a^3} \tag{3}$$

Assuming radiation in a free field, acoustic dipole sound power is given by

$$\Pi(\omega) = \frac{1}{3}\,\frac{p_F^2(\omega)}{\rho a}\,(4\pi r^2) \tag{4}$$

Employing Eqs. (3) and (4), and replacing $\overline{|F_D^2(\omega)|}$ $p_S^2(f) \cdot A^2(f)$ finally yields

$$\left[\frac{p_F(f)}{p_S(f)}\right]^2 = \frac{9}{4}\,\frac{f^2A^2(f)}{a^2r^2} = \frac{9}{4}\,\frac{f^2\,[l_x(f)\cdot l_y(f)]^2}{a^2\ r^2} \tag{5}$$

giving the ratio of mean square far-field and surface pressure for one source element.

In applying Eq. (5) to the problem of edge noise the crucial assumption is made that the frequency-dependent relevant pressure field correlation area $A(f)$ can indeed be measured on the trailing edge. It should be re-emphasized that Eq. (5) is strictly valid for source dimensions much smaller than the radiated wavelength. Taking an average value of both the lateral and longitudinal correlation lengths as $l_{x,y} = 0.5\ U_\infty/f$, then $k \cdot l_{x,y} = 0.5(2\pi f/a)\ (U_\infty/f) \ll 1$ for Mach numbers much smaller than 0.32. This condition is approximately satisfied, since glider flight speeds (and, typical landing approach speeds, for that matter) are in the Mach number range of $0.2 \leq M_\infty \leq 0.25$.

Not having measured surface pressure fluctuations on the lower flap side should not be considered a serious omission. Mugridge,[8] for example, determined from wind tunnel experiments that fluctuating pressure levels on the upper surface exceeded those on the lower surface by about 10 dB. Thus, the signal strength is evidently entirely determined by upper surface flow, with no problem from possible correlations between the upper and lower pressure field. Hence, it should suffice to take data on the upper surface only to determine the signal strength from an aircraft wing flap.

Having available all required input quantities, in particular trailing-edge surface pressure spectra (see Fig. 7), longitudinal (see Fig. 9) and lateral (see Fig. 10) correlation lengths, the validity of Eq. (5) can be checked. The following two suppositions were made: 1) the total radiating trailing-edge area is represented by $n = Y/l_y$ incoherently radiating areas along the trailing edge¶ of extent $l_x = 0.72\ U_\infty/f$ and $l_y = 0.26\ U_\infty/f$, in the streamwise and lateral direction, respectively; and 2) the directivity of the source is that of a half-baffled dipole source. With these suppositions the following equation is obtained for the ratio of surface and far-field pressure:

$$\left[\frac{p_F(f)}{p_S(f)}\right]^2 = 0.3\frac{U_\infty^2}{a^2}\frac{U_\infty Y}{f r^2}\sin^2\left(\frac{\theta - \pi/2}{2}\right) \qquad (6)$$

The constant of proportionality in this equation is, of course, only valid for the particular case under consideration. On this basis the glider trailing-edge-related far field sound pressure level spectrum, predicted from surface pressure information (Fig. 12), shows acceptable agreement between predicted and measured spectra for the time when the glider was directly over the microphone array ($\theta = 0$). The high-frequency peak in the measured spectrum near 3 kHz is possibly due to sound radiation from the horizontal stabilizer. Alternatively, it could very well be due to some periodic vortex shedding off the trailing edge as had been observed at certain sensor locations near the flap trailing edge (see Fig. 6), assuming the sensor to be sensitive only with respect to the "upper surface" vortex shedding. The underprediction of the spectral portions above 4 kHz could be accounted for by applying a Corcos' finite transducer size correction.[9] The dashed lines in the low-frequency range represent an upper bound for the predicted far-field spectrum. In fact, for this particular prediction the previously defined limiting frequency will be close to 400 Hz, so that for lower frequencies the radiated far-field sound pressure level will decrease due to a decrease in lateral and longitudinal correlation lengths of the surface pressure field.

## Landing Gear Aeroacoustic Source Characteristics and Far-Field Radiation

The landing gear model investigated had a wheel diameter of $D = 0.27$ m. Reynolds numbers based on this diameter were of the order of one million, leading to turbulent flow separation even when the forward wheel set was impinged upon by undisturbed flow.

¶Distributing sound sources of equal strengths all along the trailing edge seems appropriate because of the large aspect ratio of the SB-10 glider wings; the wings in this context can be considered as being essentially "two dimensional."

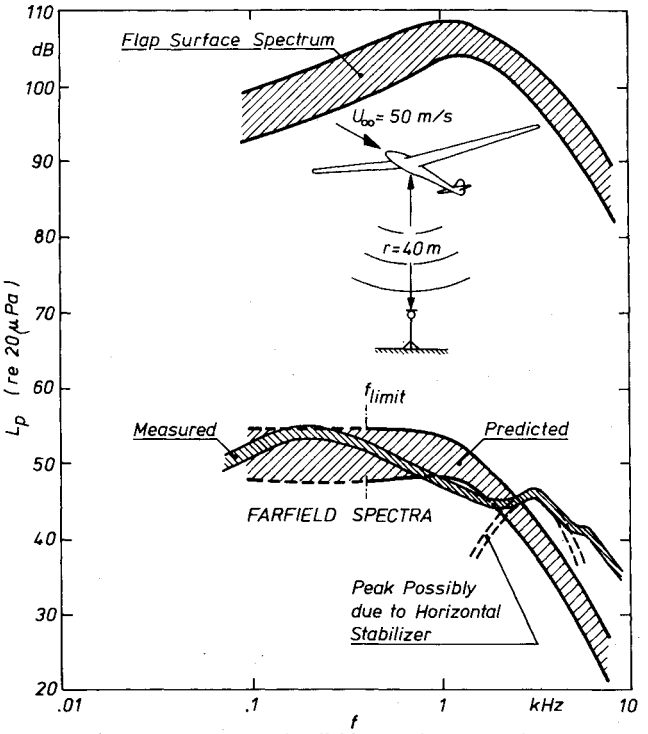


**Fig. 12 Prediction of the far-field sound spectra from surface pressure characteristics on the SB-10 wing flap trailing edge ($\theta = 0$).**

### Fluctuating Surface Pressure Data

Previous model tests[10,11] have shown that the dominant mechanism responsible for sound radiation from a four-wheel main landing gear bogie is related to turbulent flow impingement on the rear set of wheels. Four-wheel main landing gear sound generation is obviously concentrated in the region aft of the forward wheel set and all over the rear wheel set. Viewing the flow pattern (Fig. 13), it becomes quite obvious, why strong unsteady flow phenomena should occur at these locations. The turbulent wheel-flow wake is pushed downwards and inwards, resulting in violent flow patterns on the inside rear wheel with highest fluctuating pressures at these locations. A typical surface pressure spectrum measured on the inside of the rear wheel of the landing gear model is shown in Fig. 14. The data are normalized on a $p_s/q_\infty$ vs Strouhal number basis, with the wheel diameter as the relevant length dimension. Data collapse very well on this basis.

Figure 15 shows normalized surface pressure spectra at various locations on the forward and aft wheel. All spectra were measured in the inner region of the treads except spectrum (h), which pertains to the outer region and is only shown for comparison. A tentative explanation of the shapes of these spectra is as follows:

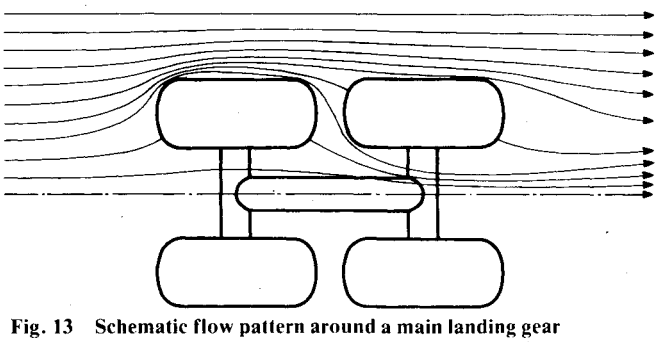

**Fig. 13 Schematic flow pattern around a main landing gear configuration.**

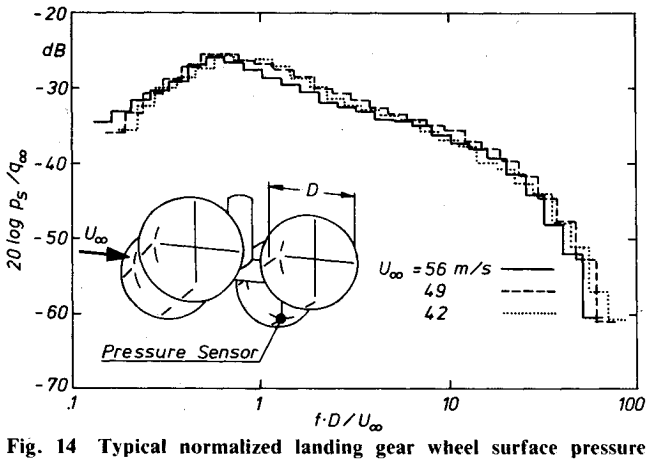


**Fig. 14 Typical normalized landing gear wheel surface pressure spectra.**

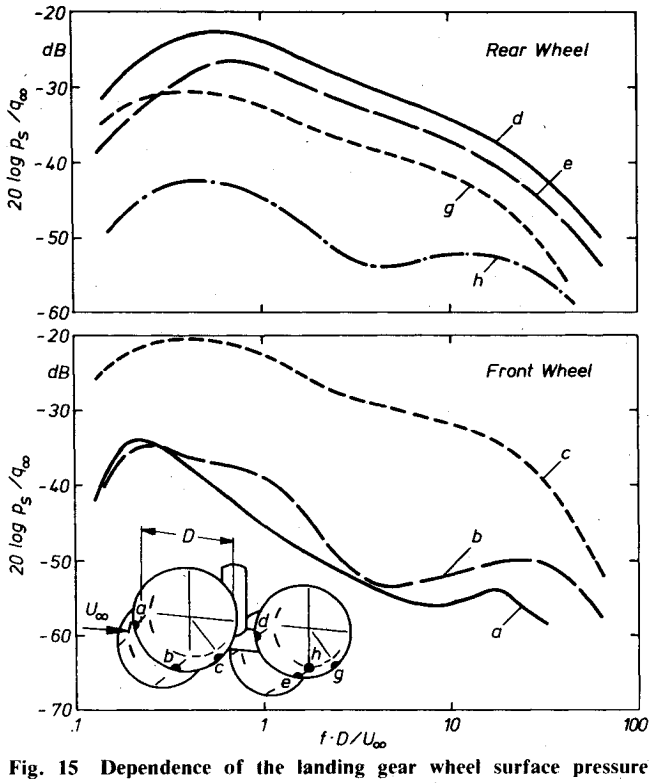


**Fig. 15 Dependence of the landing gear wheel surface pressure spectra on flow conditions at the measuring point.**

Spectra (a) and (b), measured within an area of laminar boundary-layer conditions represent some kind of "background spectra" exhibiting a few weak peaks—eliminated in the figure—which cannot be normalized on a Strouhal number basis and might be due to vibration effects.

Spectrum (c) shows high intensity levels of broadband character due to flow separation in the vicinity, or upstream, of the sensor location.

Spectra (d), (e), and (g) are of similar character indicating the impingement of flow shed off the forward wheel. The significant level drop in the flow direction shows the decrease of turbulence by flow acceleration around the wheel.

Spectrum (h) measured in the outer region of the tread can be compared with spectra (a) and (b). As shown in Fig. 13, this portion of the aft wheel is not impinged upon by flow shed off the forward wheel, resulting in comparatively low fluctuation-pressure levels.

### Source Considerations

While sound radiation from a wing trailing edge can be considered to be the result of "two-dimensional" flow

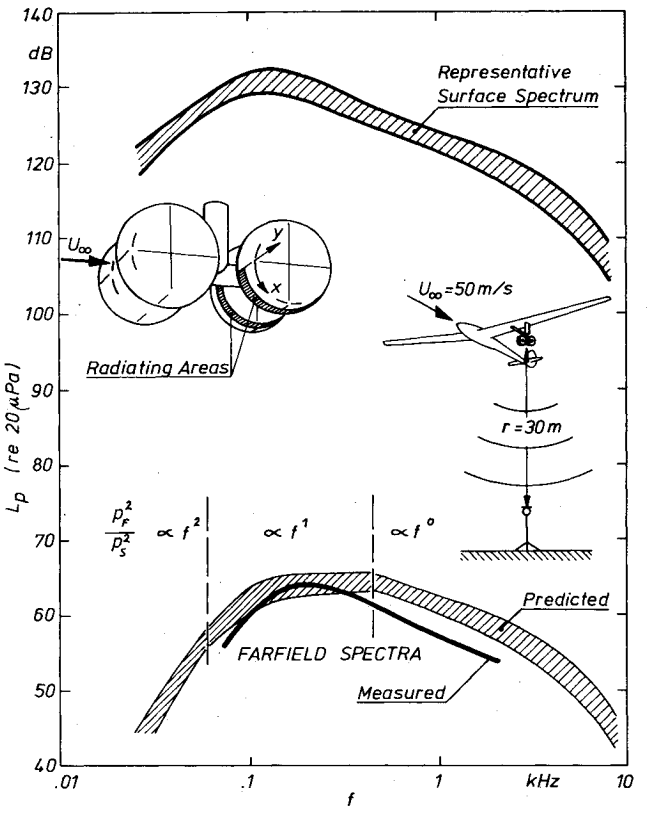


**Fig. 16 Prediction of the far-field sound spectra from surface pressure characteristics on landing gear aft wheels ($\theta = \Pi/2$).**

phenomena, a landing gear causes the flow to assume complicated three-dimensional patterns. Thus, the typical acoustic wavelength and the hydrodynamic wavelength at frequencies near the spectral maximum are both of the order of the body (i.e. landing gear) dimensions. In this regime, one would expect "whole-body-dipole" sound radiation.

The fluctuating pressures, measured on the wheels—as shown in Figs. 14 and 15—could thus not be considered representative for "isolated patches" on the gear, but rather as representative for the entire bluff body (specifically the rear set of wheels and axles). Large correlated turbulent regions shed from the forward wheel set cause reactive forces to occur on the rear set of wheels of order $p_S \cdot A$, where $p_S$ is the measured surface fluctuating pressure and $A$ is a representative correlated surface pressure area on the wheel surface, responsible for the radiation of sound.

### Prediction of Far-Field Radiation from Landing Gear Surface Pressure Characteristics

In order to relate surface spectra to radiated far-field pressure spectra in this aerodynamically complex case, the basic approach was used, somewhat arbitrarily taking for both the lateral and longitudinal correlation lengths a value of $l_x = l_y = 0.5\ U_\infty/f$. Assuming the prime radiating area to be the inner portions of the rear treads (identified in Fig. 16 through crosshatching) that are impinged upon by the flow shed from the forward wheels, a far-field spectrum was predicted and compared with the measured far-field spectrum (Fig. 16).

The agreement of predicted and measured spectrum is surprisingly good. It should be emphasized that the somewhat arbitrary assumption of the correlation lengths does not have much effect on the prediction.

Applying the analytical expression, one finds that in the high-frequency region, far-field and surface pressure spectra have a $f^0$ dependence (i.e., their shapes are identical). At a frequency where the lateral correlation length becomes equal to half the width of the wheel, one finds a $f^1$ dependence.

Finally, where the longitudinal correlation length becomes equal to that portion of the circumferential length—which is considered as radiating—there is a $f^2$ dependence.

The overprediction for high frequencies, where correlation lengths become small with respect to the body dimensions, might be due to cancellation effects of areas of correlated pressure fluctuations, an effect similar to infinite boundary-layer flow conditions.

## Conclusions

### Wing Trailing-Edge Sources

Employing a high-performance glider as a primary test vehicle, the feasibility has been demonstrated to: 1) determine the characteristics of the relevant aeroacoustic sources (in terms of fluctuating pressure spectra and pressure field correlation characteristics) of trailing-edge noise under realistic flight conditions; and 2) deduce the radiated acoustic far-field from such sources. Although it can and will not be firmly stated that an aircraft wing under flight conditions generates sound purely through edge-located sources, there is strong indication that other potential sources, such as the lower wing surface turbulent boundary layer, are in fact, of lesser importance. Since a glider wing has no high-lift devices (such as multislotted trailing-edge flaps, which in powered aircraft represent important sound sources), trailing-edge sources can be specifically and usefully studied with no non-trailing-edge-related sources to interfere.

The simple analytical model employed to predict trailing-edge noise from measured source characteristics, that assumed the prevalence of mutually uncorrelated sources located along the wing trailing-edge span, satisfactorily predicted far-field measured noise. Thus, there is strong indication that the wing trailing edge is one of the dominant sources of aircraft airframe noise.

### Landing Gear Sources

Using an aerodynamically clean glider to carry fairly large models of four-wheel landing gears, it was possible to obtain sufficient signal-to-noise ratio to clearly identify the landing gear related far-field spectra within the entire radiated airframe noise spectrum. By systematically mapping fluctuating surface pressure spectra at appropriate locations on the wheel surfaces—specifically in areas of turbulent flow impingement, or areas of flow separation—regions of particularly high fluctuating pressure levels were identified. Postulating these regions to be potential sources of landing gear related noise, the application of a fairly simple analytical model to relate surface pressure spectra and far-field radiated noise verified the region aft of the forward wheel set and the forward and downward portion of the aft wheels as the primary sources, since predicted and measured landing gear noise showed acceptable agreement. Furthermore, results from a companion study[12] conclusively show that wheelwell related aeroacoustic sources are of negligible importance in airframe noise.

## Acknowledgments

The authors would like to thank the Akademische Fliegergruppe (Akaflieg) in Braunschweig, Germany, for making their SB-10 glider available. The proficiency of the Akaflieg pilots substantially contributed to the success of the experimental program.

## References

[1] *Jane's, All the World's Aircraft,* Jane's Yearbooks, London, England, 1973/74.

[2] Hahn, M., "Turbulent Boundary-Layer Surface-Pressure Fluctuations near an Airfoil Trailing Edge" AIAA Paper 76-335, San Diego, Calif., 1976.

[3] Panton, R.L., "Theoretical and Flight Test Study of Pressure Fluctuations under a Turbulent Boundary Layer, Part 2: Flight Test Study" NASA CR-140448, 1974.

[4] Schloemer, H.H., "Effects of Pressure Gradients on Turbulent-Boundary-Layer Wall Pressure Fluctuations," *Journal of the Acoustical Society of America,* Vol. 42, (1), 1967, pp. 93-113.

[5] Bull, M.K., "Properties of the Fluctuating Wall-Pressure Field of a Turbulent Boundary Layer," AGARD Rept. 455, Paris, 1963.

[6] Bhat, W.V., "Flight Test Measurements of Exterior Turbulent Boundary Layer Pressure Fluctuations on Boeing Model 737 Airplane," *Journal of Sound Vibration,* Vol. 14, (4), 1971, pp. 439-457.

[7] Morse, P.M. and Ingard, K.U., *Theoretical Acoustics,* McGraw-Hill, New York, 1968.

[8] Mugridge, B.D., "Acoustic Radiation from Aerofoils with Turbulent Boundary Layers," *Journal of Sound and Vibration,* Vol. 16, (4), 1971, pp. 593-614.

[9] Corcos, G.M., "Resolution of Pressure in Turbulence," *Journal of the Acoustical Society of America,* Vol. 35, (2), 1963, pp. 192-199.

[10] Heller, H.H. and Dobrzynski, W.M., "Sound Radiation from Aircraft Wheel-well/Landing Gear Configurations," AIAA Paper 76-552, Palo Alto, Calif., 1976.

[11] Dobrzynski, W.M., "Modelluntersuchungen zur Bestimmung des Lärmanteils von Flugzeugfahrwerks-Schachtkonfigurationen am Flugzeugeigengeräusch," 5, Tagung der Deutschen Arbeitsgemeinschaft für Akustik, DAGA-76, Heidelberg, 1976.

[12] Dobrzynski, W.M. and Heller, H.H., "Are Wheel-Well Related Aeroacoustic Sources of any Significance in Airframe Noise?," AIAA Paper 77-1270, Atlanta Ga., 1977.